

Shear deformation of polycrystalline wadsleyite up to 2100 K at 14–17 GPa using a rotational Drickamer apparatus (RDA)

Takaaki Kawazoe,^{1,2} Shun-ichiro Karato,¹ Jun-ichi Ando,³ Zhicheng Jing,¹ Kazuhiko Otsuka,¹ and Justin W. Hustoft¹

Received 1 November 2009; revised 9 February 2010; accepted 13 April 2010; published 25 August 2010.

[1] Shear deformation experiments on polycrystalline wadsleyite (water content, ~200–2200 H/10⁶ Si) have been conducted at 14.4–17.0 GPa, 1690–2100 K, and strain rates of 2.6–16 × 10⁻⁵ s⁻¹ using a rotational Drickamer apparatus (RDA) at a synchrotron facility. The stress was measured from the orientation dependence of lattice spacing for the (013), (211), (141), (240) and (244) planes. On the basis of the mechanical and microstructural observations, we infer that deformation occurs by exponential creep through the Peierls mechanism at relatively low temperatures of 1690–2030 K. However, a sample deformed at the temperature of 2100 K showed significant grain-size reduction, and most of small grains are dislocation-free, although sub-boundaries were observed in some grains in the sample. We interpret these observations as evidence for dynamic recrystallization and that diffusion creep (and grain boundary sliding) plays an important role after dynamic recrystallization caused by power law creep. Consequently, the strength observed in the high-temperature conditions determined by the present study provides an important constraint on strength of diffusion creep and a lower limit for that of the power law dislocation creep. We conclude that the strength of wadsleyite in the power law dislocation creep is higher than or comparable to that of olivine and the strength of wadsleyite in the Peierls regime is similar to that of olivine.

Citation: Kawazoe, T., S. Karato, J. Ando, Z. Jing, K. Otsuka, and J. W. Hustoft (2010), Shear deformation of polycrystalline wadsleyite up to 2100 K at 14–17 GPa using a rotational Drickamer apparatus (RDA), *J. Geophys. Res.*, *115*, B08208, doi:10.1029/2009JB007096.

1. Introduction

[2] Wadsleyite is the most abundant mineral in the upper part of the mantle transition zone from 410 km to ~500 km depth. The knowledge of its rheological properties is essential to understanding the mantle dynamics of that region. However, the experimental data on the creep strength of wadsleyite is limited due to the difficulties in quantitative experimental studies of plastic deformation at conditions of the upper part of the transition zone (14–18 GPa and ~1700 K). The creep strength of dry and wet wadsleyite was measured at 0–10 GPa and 298–873 K using a cubic anvil apparatus and in situ X-ray measurement through stress relaxation tests [Chen *et al.*, 1998]. However, the relevance of these results for mantle dynamics is questionable for the following reasons. First, the sample was deformed at low temperatures and pressures. These are far from the typical conditions in the transition zone. Second, wadsleyite powder

was used as a starting material, and the stress was measured using the X-ray peak-broadening method. It is difficult to estimate stress values using this method because a peak width of in situ X-ray diffraction is also affected by crushing and sintering of the powdered sample. Thurel and colleagues conducted a detailed study on the dislocation microstructures of wadsleyite deformed by a Kawai apparatus [Thurel and Cordier, 2003; Thurel *et al.*, 2003a, 2003b]. These studies have provided important insight into the possible slip systems in wadsleyite, but the deformation experiments were conducted by stress relaxation and no rheological data was obtained in this series of studies.

[3] There have been some studies on the properties of wadsleyite that are related to rheological properties. They include experimental studies on atomic diffusion [Kubo *et al.*, 2004b; Shimojuku *et al.*, 2004; Shimojuku *et al.*, 2009], grain growth rate [Nishihara *et al.*, 2006], and transformation kinetics from olivine to wadsleyite [Hosoya *et al.*, 2005; Kubo *et al.*, 2004a; Rubie and Ross, 1994]. However, the relation of these studies to plastic flow in wadsleyite is rather indirect.

[4] Recently, the creep strength of wadsleyite was examined up to 1800 K at 15–16 GPa using the rotational Drickamer apparatus (RDA) [Nishihara *et al.*, 2008]. The results are the first quantitative measurement on the creep strength of wadsleyite at the mantle transition zone conditions. However,

¹Department of Geology and Geophysics, Yale University, New Haven, Connecticut, USA.

²Also at Geodynamics Research Center, Ehime University, Matsuyama, Ehime, Japan.

³Department of Earth and Planetary Systems Science, Hiroshima University, Higashihiroshima, Japan.

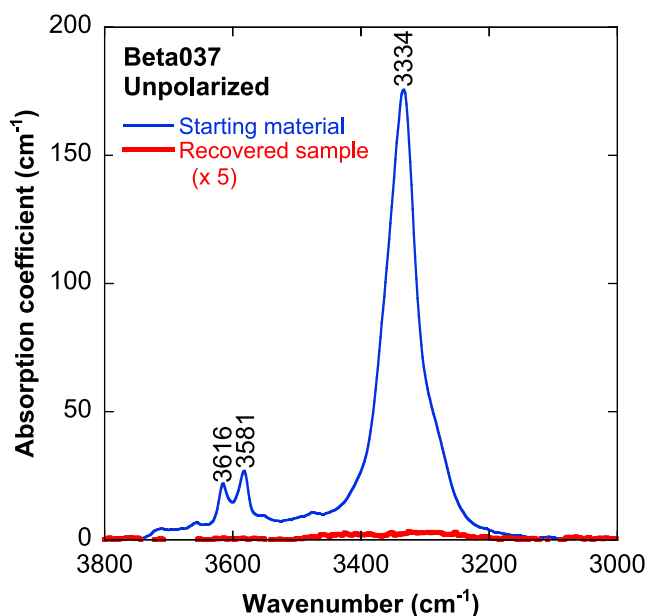


Figure 1. Unpolarized FT-IR spectra of a recovered sample and a starting material of run Beta037. Bold and thin lines are spectra of the recovered sample and of the starting material, respectively. The intensity of the absorption spectrum of the recovered sample is magnified by 5. These spectra yield the water contents of the recovered sample and the starting material as 280 H/10⁶ Si (17 wt ppm H₂O) and 36000 H/10⁶ Si (2200 wt ppm H₂O), respectively.

there are some limitations in the *Nishihara et al.* [2008] study. For example, they did not obtain strong constraints on deformation mechanisms due to the limited range of experimental conditions. The temperature conditions of their experiments may not be high enough to determine the creep strength of wadsleyite in the power law creep regime. It is likely that their samples were deformed in the Peierls regime, judging from the similar study on olivine [*Kawazoe et al.*, 2009] and in which case the applicability of those results is limited. It is important to determine the creep strength of wadsleyite in the power law creep regime at higher temperatures to obtain the rheological data that can be applied to mantle dynamics. Another point is that stress value was measured using the orientation dependence of only one lattice spacing. Because the stress determined from X-ray diffraction depends on the lattice plane from which X-ray is diffracted, it is important to determine the stress from several lattice planes.

[5] Here we report the experimental results on the creep strength of water-poor polycrystalline wadsleyite under a broader range of temperatures with an improved X-ray diffraction data. Our new results provide the first experimental data on a range of deformation mechanisms including the Peierls mechanism, power law dislocation creep, and diffusion creep.

2. Experimental and Analytical Methods

2.1. Starting Materials

[6] Polycrystalline wadsleyite aggregates were used as starting materials. Single crystals of San Carlos olivine

((Mg_{0.9},Fe_{0.1})₂SiO₄) with no inclusions visible to the naked eye were hand-picked, ground, and sorted in distilled water. The sorted San Carlos olivine powder with grain size of 3–8 μm was mixed with 1–1.5 wt % San Carlos orthopyroxene to control the activities of oxide components in the wadsleyite. Polycrystalline wadsleyite was synthesized at 15 GPa and 1370–1420 K for 1–3 h with no additional water in a Mo foil capsule using a Kawai apparatus. Water content of the starting material was determined by the Fourier transform infrared (FT-IR) spectroscopy (Figure 1) and ranges from 32,000 to 36,000 H/10⁶ Si (using the Paterson calibration, described later). Grain size of the starting material was measured using the secondary electron image (SEI) (described later) and was 3.8 or 7.9 μm.

2.2. Experimental Procedure

[7] Deformation experiments have been conducted at confining pressures of 14.4–17.0 GPa, temperatures of 1690–2100 K and $\dot{\epsilon}$ (strain rates) of 2.6–16 × 10⁻⁵ s⁻¹ using the RDA at X17B2 beam line, National Synchrotron Light Source (NSLS), Brookhaven National Laboratory (BNL), USA. The sample geometry and the cross section of a typical cell assembly are shown in Figures 2 and 3, respectively. Attention has been paid to several issues in the development of the cell assembly. First, we used a half-ring-shaped sample to minimize the variation in stress (and strain rate) within a sample because torsion tests were conducted in which stress and strain rate in a sample changed with the distance from the rotation axis. The typical sample dimensions were 1.0 and 1.6 mm in inner and outer diameters, respectively, and the thickness was 200 μm. Second, to minimize the extrusion that occurred due to compression, a sample was surrounded by a strong material (Al₂O₃). Third, to minimize the absorption of X-ray along the path, a large portion of gasket (pyrophyllite) in the X-ray path was replaced with a polyetheretherketone (PEEK) and boron epoxy. The sample was heated using internal disk heaters made of a hot-pressed TiC-diamond composite (3:2 weight ratio). Temperature and its variation in the sample were measured by an enstatite-diopside thermometry [*Gasparik*, 1996] in runs Beta034, Beta035, and

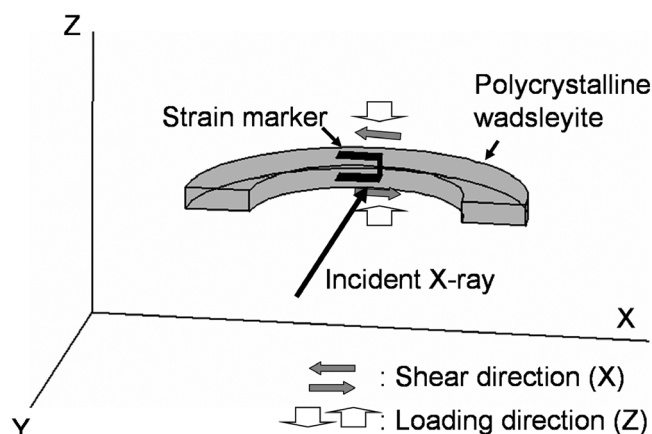


Figure 2. Sample geometry. Z is the direction of the loading. Y is the direction of X-ray beam and is normal to Z. X direction is perpendicular to both of them and parallel to the shear direction. Strain marker is placed as shown to measure shear and uniaxial strain rate.

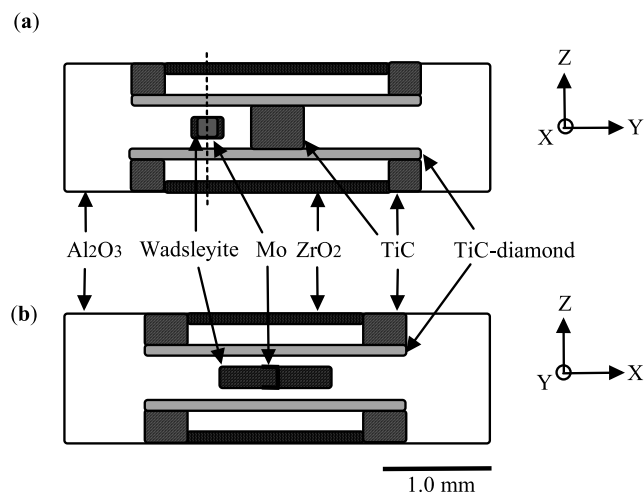


Figure 3. Cross section of the cell assembly. (a) A cross section in the Y-Z plane (cut in the center). (b) A cross section in X-Z plane (cut in the plane shown by a dashed line in Figure 3a).

Beta037. In runs Beta036, Beta039, and Beta040, sample temperature was estimated by an empirical relationship between sample temperature, cell thickness, and electrical power to the heater. We estimate the uncertainty in temperature in this study is less than ± 120 K considering uncertainties in temperature variation in the sample (less than ± 110 K) and the empirical relationship between the sample temperature, the cell thickness and the power (± 120 K).

[8] The samples were compressed to desired loads (pressures) at room temperature and then annealed at high temperatures for 65–174 min before deformation. The electric power to the heater was kept constant during annealing and deformation. Annealing is critical because a large number of defects (dislocations and fine grains) are created during the pressurization processes. The necessary annealing conditions were explored on the basis of annealing experiments in which grain size and grain boundary morphology after annealing were studied. The microstructure and water content of a recovered sample of the annealing experiments are considered to correspond to those prior to deformation in deformation experiments. An SEI of an annealed sample and a result of FT-IR measurement are shown in Figures 4 and 1, respectively. The grain boundary morphology after annealing at 15.7 GPa and 1670 K for 94 min shows near-equilibrium geometry (Figure 4). Reduction of the sample stress (to less than $\sim 1/2$ of the steady state value) after annealing was also confirmed using in situ X-ray observation which is described later. In the annealing experiment (run Beta039), the initial water content in the starting material ($36000 \text{ H}/10^6 \text{ Si}$) was reduced to $1100 \text{ H}/10^6 \text{ Si}$ (65 wt ppm H_2O) after annealing, which is comparable to those after deformation ($200\text{--}2200 \text{ H}/10^6 \text{ Si}$). After annealing, shear traction was applied to the samples under high pressure and temperature by rotating one of the tungsten carbide anvils.

[9] During deformation, deviatoric stress and strain rate in the samples were measured by means of in situ X-ray diffraction and radiography, respectively. Energy-dispersive X-ray diffraction patterns were taken using an optical system composed of an incident slit, a conical receiving slit, and a

multielement solid-state detector. White incident X-rays were collimated by a $50 \times 50 \mu\text{m}^2$ or a $100 \times 100 \mu\text{m}^2$ slit, and the width of a conical receiving slit was $50 \mu\text{m}$. Diffracted X-rays were taken at four different azimuth angles of 0° , 30° , 60° , and 90° typically for 15 min. Using Al_2O_3 powder as a standard material, 2θ angles for the four elements were determined and ranged from 6.498° to 6.517° that depends on each detector and run with an error of $\pm 0.001^\circ\text{--}0.003^\circ$ for each detector for a given run. Stress values were calculated from the observed azimuth dependence of d spacings of wadsleyite peaks, (013), (211), (141), (240) and (244). X-ray radiograph of the strain marker was taken using an yttrium-aluminum-garnet crystal and a CCD camera. Detailed description of the in situ measurements of stress and strain at the X17B2 beam-line can be found elsewhere [Chen *et al.*, 2004]. With our diffraction geometry, the volume from which diffracted X-ray is collected to the detector has an elongated shape [Xu *et al.*, 2005], and the stress values are the average stress from a sample region ranging from the inner to the outer part. Since a sample is deformed by torsion, stress varies from the inner to the outer region of a sample. With the ring-shaped sample, the variation in stress in a sample is $\sim 8\%$ for the stress exponent n of 3.5.

[10] We used a model of stress versus lattice strain relationship [Singh, 1993] with a modification to more general stress geometry that includes both uniaxial compression and simple shear [Xu *et al.*, 2005]:

$$d_{hkl} = d_{hkl}^0 \left[1 + \frac{\sigma_U}{6G} (1 - 3 \cos^2 \psi) - \frac{\sigma_S}{2G} \sin \psi \cos \psi \right], \quad (1)$$

where d_{hkl} is the d-spacing measured as a function of azimuth angle ψ , d_{hkl}^0 is the d-spacing under the hydrostatic pressure, G is the shear modulus, σ_U is the uniaxial stress, σ_S is the deviatoric stress. We adopt the shear modulus of polycrystalline wadsleyite determined by ultrasonic measurements at high pressure and temperature [Li *et al.*, 2001]. The stresses and d_{hkl}^0 were determined by fitting the observed d_{hkl} to equation (1) using the least squares method. Peak positions of

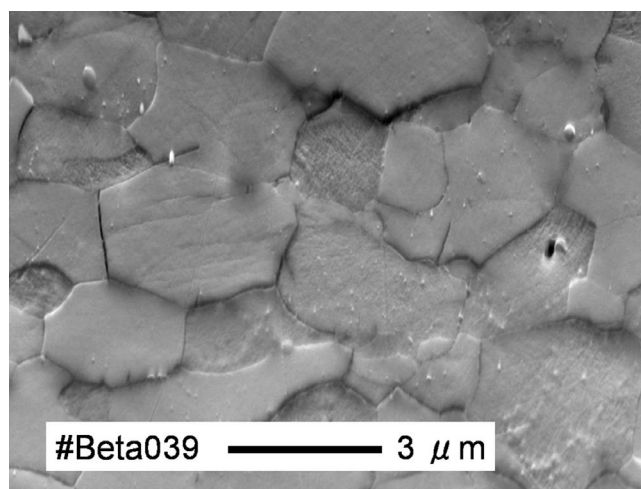


Figure 4. The secondary electron image of the sample annealed at 15.7 GPa and 1670 K for 94 min (run Beta039). The sample was sectioned in X-Z plane and etched by 35% HNO_3 . The average grain size is $3.1 \mu\text{m}$, and the grain boundary geometry suggests nearly equilibrium morphology.

X-ray diffraction and their uncertainties were determined by using PeakFit software (SeaSolve Software Inc.), and the error represents 1 standard deviation. Uncertainty of the peak position was propagated to that of the stress using equation (1). Pressure was calculated using the equation of state of wadsleyite [Fei *et al.*, 1992] and the unit cell volume was calculated using the d_{hkl}^0 . Uncertainty of the pressure originates from that of the unit cell volume and its variation during deformation.

[11] Strains and strain rates in both shear and uniaxial directions were measured by the X-ray radiographs of the strain marker and calculated using the following equations, respectively:

$$\dot{\epsilon}_S = \frac{1}{2h} \frac{\partial w}{\partial t} \quad (2)$$

$$\dot{\epsilon}_U = -\frac{1}{h} \frac{\partial h}{\partial t}, \quad (3)$$

where $\dot{\epsilon}_S$ and $\dot{\epsilon}_U$ are the shear and uniaxial strain rates, respectively, w is the displacement in shear direction, h is the height of the sample, and t is the time. The $\dot{\epsilon}_S$ changes with the distance from the rotational axis because torsion tests were conducted in this study. Inner and outer radii from the center (rotational axis) in the recovered sample were 0.72–0.80 and 1.17–1.37 mm, respectively. This difference in radii leads to the difference of the $\dot{\epsilon}_S$ between inner and outer parts of the samples to be less than $\pm 30\%$. On the other hand, uncertainties of w and h were $\pm 0.3 \mu\text{m}$ and $\pm 3 \mu\text{m}$, respectively, and these uncertainties result in uncertainty in $\dot{\epsilon}_S$ as less than $\pm 20\%$.

[12] In principle, results from the RDA can be analyzed for shear and compressional deformation separately, but considering the large uncertainties in the current stress-strain measurements, we make a simplifying assumption that plastic properties of our samples are isotropic. Under this assumption, we can analyze the results in terms of Levy-von Mises formulation of nonlinear rheology [Odqvist and Hult, 1962], i.e.,

$$\dot{\epsilon}_E = A \cdot \sigma_E^n, \quad (4)$$

where $\dot{\epsilon}_E$ and σ_E are the von Mises equivalent strain rate and stress defined by

$$\dot{\epsilon}_E = \sqrt{\dot{\epsilon}_U^2 + \frac{4}{3}\dot{\epsilon}_S^2} \quad (5)$$

$$\sigma_E = \sqrt{\sigma_U^2 + \frac{3}{4}\sigma_S^2}. \quad (6)$$

The difference of $\dot{\epsilon}_S$ due to the geometry is adopted as the uncertainty of $\dot{\epsilon}_E$ in this study because the difference is larger than that estimated from the uncertainties of w and h . This variation in strain rate causes a variation in stress of $\sim 8\%$ assuming the stress exponent n of 3.5.

2.3. Microstructures and Water Content

[13] Microstructures of the recovered samples were observed with a transmission electron microscope (TEM)

(JEM-2010 at N-BARD of Hiroshima University) and the SEI using a field-emission scanning electron microscope (SEM, XL-30 ESEM-FEG). TEM foils were prepared using the focused ion beam system (FIB, JEM-9310FIB at Geodynamics Research Center of Ehime University). The average grain sizes of the recovered sample (run Beta039) and the starting materials were calculated from the SEIs of the samples using the intercept method, and a correction factor of the sectioning effect of 1.56 is used [Mendelson, 1969].

[14] Water contents in the recovered samples and the starting materials were determined using the FT-IR spectroscopy. The samples were polished at double sides and kept in a vacuum oven at 383–423 K for more than 12 h before measurements. IR spectra were taken with unpolarized light and an aperture of $40 \times 40 \mu\text{m}^2$. Water contents were calculated using the Paterson calibration [Paterson, 1982] and density factors of $4.08 \times 10^4 \text{ L/mol}$ and $2.50 \times 10^3 \text{ L/g}$ for water contents in $\text{H}/10^6 \text{ Si}$ and wt ppm H_2O , respectively. The density factors are defined as $10^6 \times \text{M/d}$ and $9 \times 10^6/\text{d}$ for water contents in $\text{H}/10^6 \text{ Si}$ and wt ppm H_2O , respectively, where M is the molar mass in g/mol and d is the mineral density in g/L .

3. Results

[15] The experimental conditions and results are summarized in Table 1. One annealing experiment (run Beta039) was conducted at 15.7 GPa and 1670 K for 94 min to compare microstructure, grain size, and water content of the annealed sample with those of the deformed samples. The microstructure, grain size, and water content of the sample recovered from the annealing experiments are considered to correspond to those prior to deformation in the deformation experiments.

3.1. Mechanical Observations

[16] X-ray diffraction patterns were taken at four different azimuth angles to determine the stresses in the samples (Figure 5). In this study, we used the diffraction from up to five different crystallographic planes. The values of d spacing of each lattice plane depend on the orientation of each plane with respect to the macroscopic reference frame (i.e., macroscopic stress orientation). We used equation (1) to determine stresses and pressure (Figure 6). In general, the amplitude of the diffraction peaks of wadsleyite was smaller than those from the corundum pressure medium and the TiC-diamond heater. Consequently, to reduce the uncertainties due to peak overlap, we used deconvolution to separate peaks from wadsleyite from those by other materials. Several wadsleyite peaks were identified and used to determine the stress. Accuracy of the stress measurement for each diffraction peak is listed as uncertainty of the determined stress in Table 1. The stress values determined from the (240) peak were calculated with uncertainties smaller than those of the other wadsleyite peaks due to the smaller uncertainty of the position of the (240) peak. Stress-strain curves are shown in Figure 7. The deviatoric stress σ_S reached steady state at $\sim 10\%$ equivalent strain at 14.4–17.0 GPa and 1690–2100 K. The stress at steady state decreased with increasing temperature (Figure 7b).

[17] Two deformation regimes are recognized on the basis of the temperature dependence of stress at steady state

Table 1. Experimental Conditions and Results^a

	Beta037	Beta034	Beta035	Beta036-1	Beta036-2	Beta040	Beta039
Pressure ^b (GPa)	17.0 (0.8)	14.4 (0.8)	14.7 (0.8)	15.4 (1.2)	15.6 (1.1)	15.1 (0.7)	15.7 (1.0)
Temperature ^b (K)	2100 (100)	2020 (110)	2030 (100)	1930 (120)	1930 (120)	1690 (120)	1670 (120)
Equivalent strain rate ^b (10^{-5} s^{-1})	3.8 (1.1)	2.8 (0.8)	2.6 (0.8)	5.7 (1.7)	16 (5)	3.1 (0.9)	–
Equivalent strain (%)	32 (11)	40 (14)	65 (23)	70 (24)	209 (72)	19 (7)	–
Equivalent stress ^b (GPa)							
(013)	1.0 (0.6)	–	–	–	–	3.0 (0.9)	–
(211)	1.2 (0.3)	–	–	–	–	2.3 (0.6)	–
(141)	0.7 (0.2)	1.5 (0.5)	2.1 (0.3)	1.5 (0.6)	2.1 (0.6)	2.5 (0.5)	–
(240)	0.8 (0.2)	1.9 (0.5)	2.9 (0.2)	2.4 (0.4)	3.3 (0.6)	2.5 (0.2)	–
(244)	0.9 (0.4)	–	2.5 (0.4)	2.3 (0.3)	3.5 (0.4)	2.5 (0.3)	–
Average	0.9	1.7	2.5	2.1	3.0	2.6	–
Water content (H/10 ⁶ Si)							
Recovered sample	280	2200	920	–	200	380	1100
Starting material	36000	32000	32000	32000	32000	32000	36000
Grain size (μm)							
Recovered sample	5	10	10	–	10	10	3.1 (0.5)
Starting material	0.5–1	<1	<1	–	<1	<1	–
Starting material	3.8 (0.5)	7.9 (1.2)	7.9 (1.2)	7.9 (1.2)	7.9 (1.2)	7.9 (1.2)	3.8 (0.5)

^aThe numbers in parentheses indicate standard deviation.

^bDuring steady state deformation.

deformation and on the microstructural observations. The σ_E calculated using different (hkl) planes at the steady state deformations are plotted against temperature in Figure 8. At relatively low temperature ($< \sim 2000$ K) and high-stress conditions, σ_E does not change with temperature within the uncertainty. On the other hand, σ_E decreases significantly with increasing temperature at relatively high temperatures (~ 2100 K) and low stresses.

3.2. Microstructures and Water Content

[18] Figure 4 shows a microstructure of an annealed sample, which would represent the microstructure of a sample before deformation. The average grain size is $3.1 \mu\text{m}$, and grain-boundary morphology shows nearly equilibrium structure.

[19] Grain size and morphology of grain boundary of deformed samples are distinct from those of the annealed sample (Figure 9). In the samples deformed at relatively low

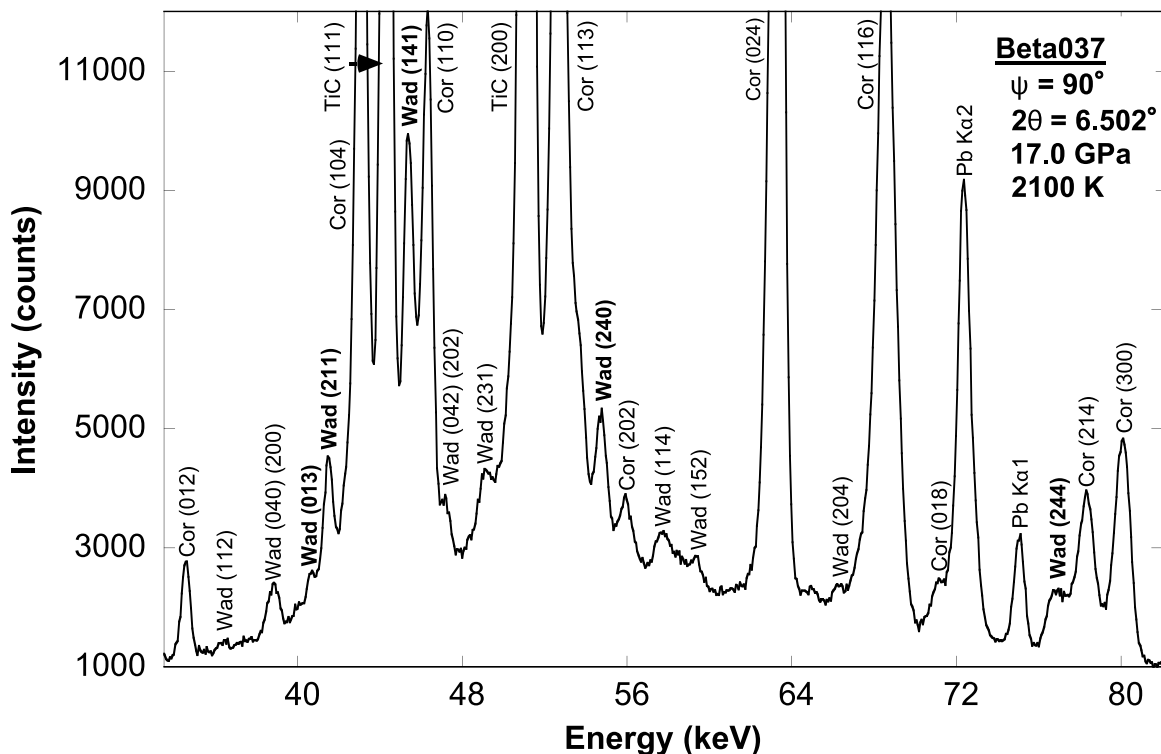


Figure 5. A representative energy-dispersive X-ray diffraction pattern of wadsleyite collected at $\psi = 90^\circ$ (horizontal diffraction) at 17.0 GPa and 2100 K during deformation (run Beta037). Wadsleyite (Wad) peaks were observed as well as diffraction peaks from corundum (Cor) pressure medium and TiC electrode.

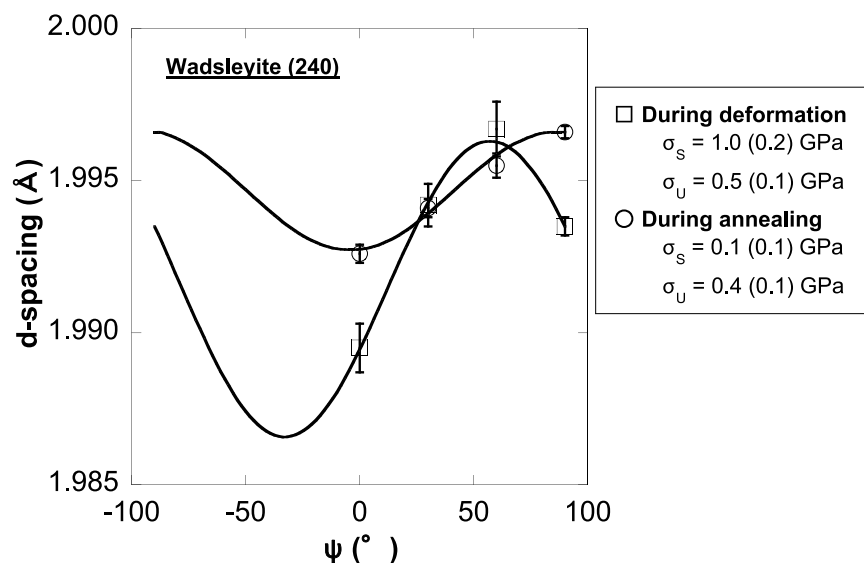


Figure 6. Two sets of results showing the variation in d-spacing of wadsleyite (240) with the azimuth angle ψ during deformation (squares) and annealing (circles) in run Beta037. Curves are derived by the least squares fitting of the d spacings to equation (1). Obtained stress values are shown in this figure with experimental conditions. Note that the maximum of the curve during deformation is close to 45° . This means that stress condition in the sample is close to simple shear.

temperatures (runs Beta034, Beta035, Beta036, and Beta040), grains are flattened and grain boundaries are serrated. Grain size is bimodal and portions around larger relict grains ($\sim 10 \mu\text{m}$) are occupied by smaller grains ($< 1 \mu\text{m}$), suggesting only limited recrystallization. In contrast, in the sample deformed at the highest temperature (Beta037, deformed at 2100 K), a large portion of the sample is occupied by nearly homogeneous grains smaller than the starting grain size ($\sim 0.5\text{--}1 \mu\text{m}$), although some regions show a mixture of large relict grains ($\sim 4\text{--}6 \mu\text{m}$) with smaller grains ($< 1 \mu\text{m}$). We interpret that this high temperature sample (Beta037) shows evidence of more extensive dynamic recrystallization.

[20] TEM observations of the recovered samples indicate that the microstructures strongly depend on the experimental temperature. At the lower temperature conditions (runs Beta034, Beta035, and Beta036, deformed at 1930 K to 2030 K), dislocation cell structures are formed within larger relict single crystals that are composed of walls separating subgrains with heavily tangled dislocations (Figure 10). Misorientations between adjacent cells are small ($< 5^\circ$) and the size of the cell is $\sim 200\text{--}500 \text{ nm}$. The tangled dislocations are also observed within the each cell. The presence of the heavily tangled dislocation causes the bend of crystallographic orientation which makes it difficult to operate the weak-beam dark field (WDF) method. The straight free dislocations can be clearly imaged by WDF, only within a cell with lower dislocation density, which is $\sim 2 \times 10^{14} \text{ m}^{-2}$ (Figure 10c). This value should be the minimum dislocation density of the sample. This dislocation density suggests stress magnitude as high as several GPa in the sample according to relationship between stress and dislocation density (to estimate the stress value, we used the relationship after normalizing that of olivine [Karato and Jung, 2003] by using shear modulus of olivine and wadsleyite). It is difficult to estimate

the stress value in the wadsleyite sample because the relationship between stress and dislocation density of wadsleyite has not been determined so far. The estimated stress is, however, approximately consistent with the mechanical observation.

[21] At the higher temperature condition (run Beta037, deformed at 2100 K), a portion composed of fine grains ($\sim 0.5\text{--}1 \mu\text{m}$) is observed in the recovered sample with some bimodal regions composed of large relict grains ($\sim 4\text{--}6 \mu\text{m}$) with smaller grains ($< 1 \mu\text{m}$). The portion of the fine grains was $\sim 40\text{--}60\%$, and the rest of the sample was composed of the relict grains with smaller grains in a cross section of the sample. Although some grains show high density of tangled dislocations similar to low-temperature samples, grains much smaller than the starting grain size ($\sim 0.5\text{--}1 \mu\text{m}$) are formed as shown in Figures 9 and 11. The difference of crystallographic orientation of these small grains is large, and many grain boundaries are straight. These facts indicate that the dynamic recrystallization occurred during experiments with substantial grain boundary migration. There are few dislocations in most of the grains, but the free dislocations and subgrain boundaries are observed in some grains (Figure 11b). Dislocation density of the grains is much smaller than those of the sample deformed at lower temperature.

[22] Water contents of deformed samples and starting materials are listed in Table 1, and representative FT-IR spectra are shown in Figure 1. The water contents in the starting materials ranged from 32,000 to 36,000 H/10⁶ Si (from 1900 to 2200 wt ppm H₂O). In the annealing experiment (run Beta039), the initial water content in the starting material (36,000 H/10⁶ Si, 2200 wt ppm H₂O) was reduced to 1100 H/10⁶ Si (65 wt ppm H₂O) after annealing, which is comparable with those after deformation ($< 2200 \text{ H/10}^6 \text{ Si}$). These results indicate that water contents in the samples were

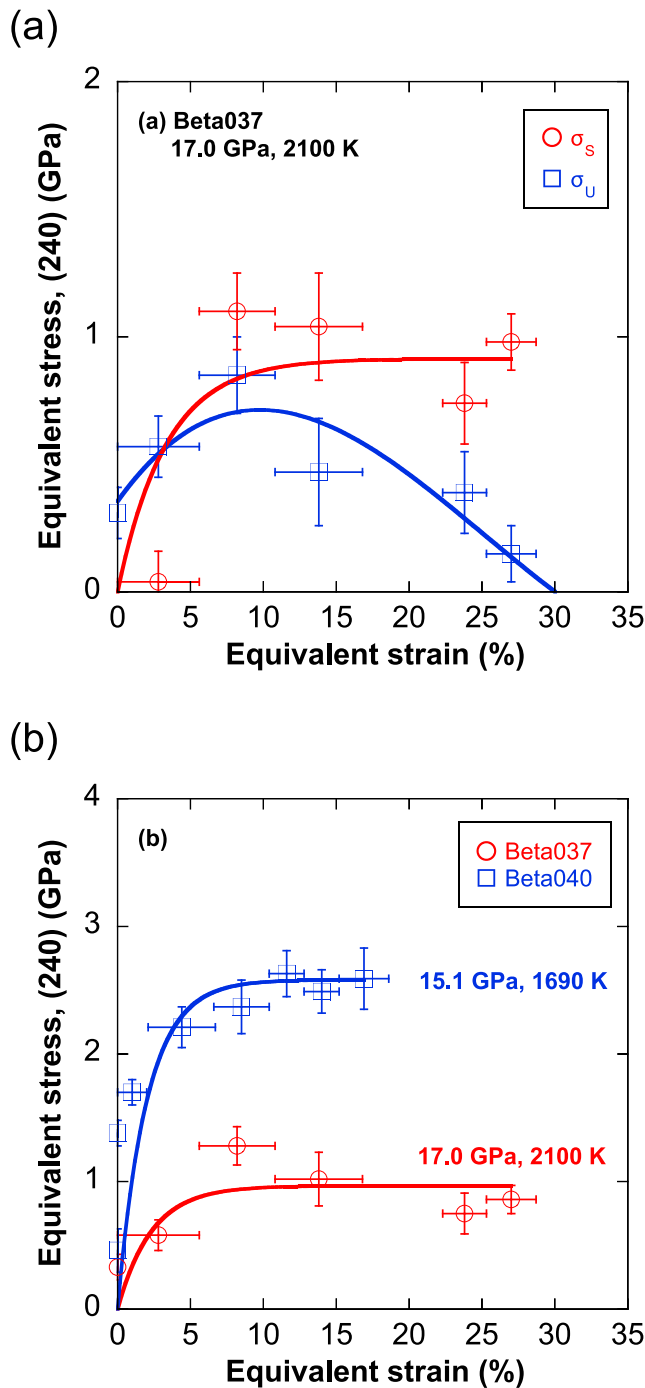


Figure 7. Stress-strain curves. (a) A comparison between shear and uniaxial stresses. Shown are those calculated using a (240) plane (run Beta037). Experimental conditions at steady state were 17.0 GPa, 2100 K, and $3.8 \times 10^{-5} \text{ s}^{-1}$. (b) A comparison of stress calculated using the (240) plane between different temperature conditions (1690 and 2100 K) at similar pressures. Steady state can be observed from equivalent strain of $\sim 10\%$.

reduced during annealing and the samples were deformed under water-poor conditions ($< 2200 \text{ H}/10^6 \text{ Si}$), although these water contents are much higher than those for comparable RDA deformation experiments on olivine [Kawazoe *et al.*, 2009].

4. Discussion

4.1. Deformation Mechanism

[23] Three distinct mechanisms of deformation are commonly identified in silicate minerals [e.g., Karato, 2008]: the Peierls mechanism, power law dislocation creep, and diffusion creep. For a given grain size and temperature and pressure, the Peierls mechanism dominates at high stresses changing to power law creep and finally to diffusion creep at the lowest stress level. When grain size changes during deformation, further complications occur, including the possible switch to deformation by grain size sensitive creep. Each mechanism has its own signature in the flow law and microstructures.

[24] The mechanical and microstructural observations on the deformed samples suggest that the experimental conditions in our study cover these three rheological regimes as discussed later. The flow law under the conditions where both dislocation glide and climb are active is the power law equation:

$$\dot{\epsilon} = A_{PL} \sigma^n \exp\left(-\frac{H^*_{PL}}{RT}\right), \quad (7)$$

where A_{PL} and H^*_{PL} are a preexponential constant and the activation enthalpy in the power law regime, respectively, R is the gas constant, and T is the temperature. At low temperature, high-stress conditions where only dislocation glide is operative, the following exponential flow law (i.e., the Peierls mechanism) is appropriate:

$$\dot{\epsilon} = A_{PE} \exp\left[-\frac{H^*_{PE}}{RT} \left(1 - \frac{\sigma}{\sigma_P}\right)^2\right], \quad (8)$$

where A_{PE} is a constant, σ_P is the Peierls stress, and H^*_{PE} is the activation enthalpy in the Peierls regime. At high temperature, low stress and with small grain size, diffusion creep is dominant, the flow law for which can be written as follows:

$$\dot{\epsilon} = A_{DF} \frac{\sigma}{L^m} \exp\left(-\frac{H^*_{DF}}{RT}\right), \quad (9)$$

where A_{DF} is a constant, L is grain size, H^*_{DF} is the activation enthalpy of the diffusion creep, and a parameter m take a value of 1–3.

[25] To infer the appropriate flow law, we first plot the observed creep strength as a function of temperature (Figure 8). Figure 8 indicates that the data from high temperature experiments ($> \sim 2000 \text{ K}$) show a strong temperature dependence of strength that is consistent with the power law creep, whereas the data from lower temperatures show much weaker temperature sensitivity of strength, suggesting an exponential flow law.

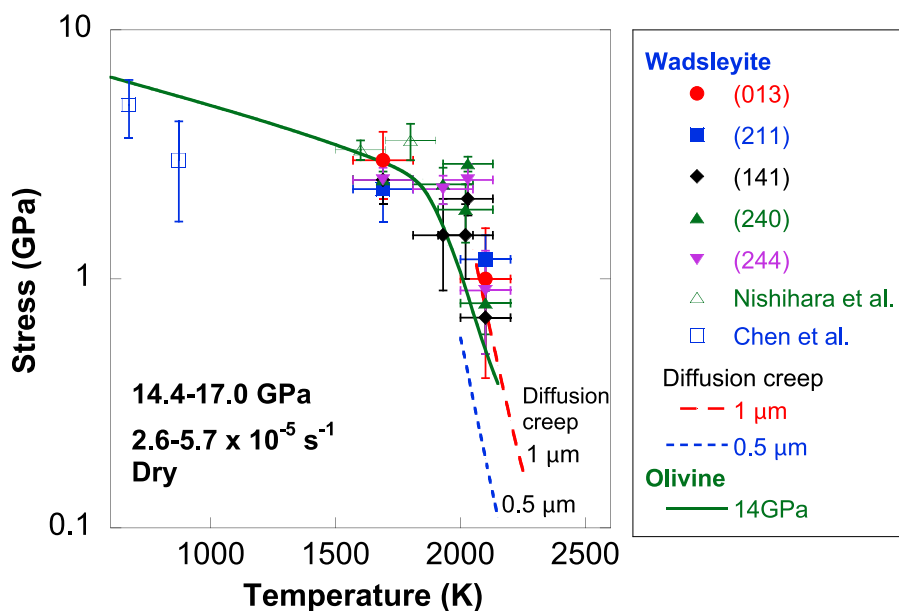


Figure 8. Creep strength of water-poor polycrystalline wadsleyite as a function of temperature (determined at 14.4–17.0 GPa and $2.6\text{--}5.7 \times 10^{-5} \text{ s}^{-1}$). Solid line is stress–temperature relationship of dry olivine at 14 GPa [Kawazoe *et al.*, 2009]. Dashed and dotted lines show creep strength in diffusion creep with grain size of 1 and 0.5 μm , respectively, which are estimated according to atomic diffusion data of wadsleyite [Shimozuku *et al.*, 2009].

[26] The TEM observation shows tangled dislocations with high density in the large grains of the sample deformed at relatively low temperatures. The microstructures in the lower temperature samples are characterized by the formation of dislocation cell structures that are composed of heavily tangled dislocation walls. In general, the tangling of dislocation occurs under the condition where dislocation climb is prohibited. Therefore, this microstructure suggests that the deformation at the lower temperatures involves only dislocation glide without much effects of recovery. Control by dislocation glide over the Peierls potential (the Peierls mechanism) is a possible mechanism of creep in this regime, which is consistent with the observed weak sensitivity of the creep strength on temperature. In addition, the observation of partial recrystallization indicates that deformation occurred by dislocation creep. Thus, for samples deformed at relatively high stresses and low temperatures, the most appropriate deformation mechanism is an exponential dislocation creep corresponding to the Peierls mechanism.

[27] The microstructures of a high temperature sample are markedly different from those of low-temperature samples. Although some grains show high density of tangled dislocations similar to low-temperature samples, there is clear evidence of recovery and/or recrystallization. These observations imply that recovery processes involving either dislocation climb or grain boundary migration or both are operative under high temperature conditions. The appropriate flow law for mechanisms involving these processes is the power law creep. This conclusion is consistent with the observed high sensitivity of the creep strength on temperature. However, the exact mechanisms of deformation are not clear. On the one hand, many recrystallized grains show very low dislocation density, suggesting that these portions of the sample may have deformed by diffusion creep or grain

boundary sliding. However, the degree to which these grain size sensitive mechanisms may control the creep strength in our samples is not clear. If the influence of grain size sensitive creep caused by fine recrystallized grains were large, then one would expect strain softening. There is no clear evidence for strain softening from our mechanical data (see Figure 7). On the other hand, the evidence of dynamic recrystallization means that deformation did occur by dislocation creep at least in the early stage of deformation. So, we conclude that deformation mechanism in the high-temperature regime is power law dislocation creep with some influence of grain size sensitive mechanisms caused by dynamic recrystallization, but the degree to which grain size sensitive creep contributes to the strength is unknown from the present work. Combined with the mechanical data showing a marked difference between the low-temperature and the high-temperature regimes, we conclude that deformation mechanisms are different between these two regimes.

[28] Thurel and Cordier [2003] and Thurel *et al.* [2003a] conducted the stress relaxation tests using a Kawai apparatus and conducted detailed TEM analyses of their samples. The dislocation structures that they reported are quite distinct from those of ours. First, the dislocation density in their samples is much smaller than ours, and their samples are well recovered. This difference is due to the fact that their deformation experiments are stress relaxation, in which the initial stress caused by cold compression ($\sim 1\text{--}3$ GPa [Karato and Rubie, 1997]) is relaxed after heating, leading to a much smaller stress (~ 0.1 GPa or so) toward the end of an experiment. Because of this temporal variation in stress, the interpretation of observed dislocation structures is complicated. In contrast, the experimental procedure by the RDA is in principle better defined; that is, we can investigate the steady state creep law and microstructures. However, currently, the

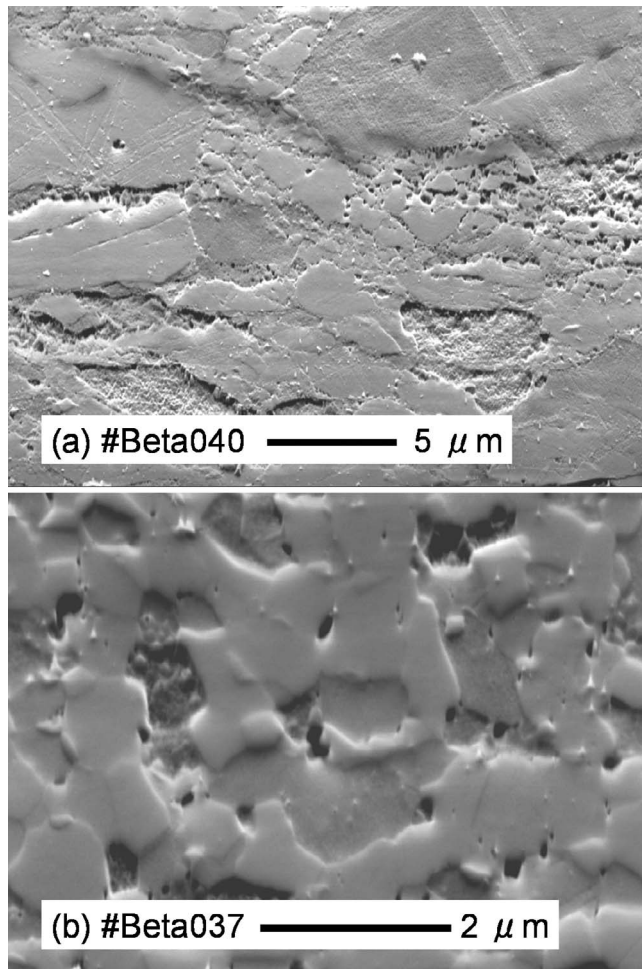


Figure 9. Secondary electron images of deformed samples. (a) A sample deformed at 1690 K, 15.1 GPa, and $3.1 \times 10^{-5} \text{ s}^{-1}$ (run Beta040). Bimodal grain sizes are observed as a result of limited dynamic recrystallization. (b) The recrystallized part of the sample deformed at 2100 K, 17.0 GPa, and $3.8 \times 10^{-5} \text{ s}^{-1}$ (run Beta037). The samples were sectioned in X-Z plane and etched using 35% HNO_3 . The shear (X) direction is horizontal.

temperature and strain rate conditions are limited and the stress magnitudes in the current experiments are still too high to allow any detailed analyses of dislocation structures. Therefore, the application of our results to the dynamics of mantle transition zone needs to be made with caution. Experimental studies under lower stresses (i.e., higher temperature, smaller grain sizes, slower strain rates, and various water contents) will be critical to obtain data that are applicable to Earth's transition zone with more confidence.

4.2. Comparison of Creep Strength With Previous Studies

[29] Creep strength for diffusion creep of wadsleyite was estimated using the atomic diffusion data in wadsleyite [Shimojuku *et al.*, 2009] and grain size and strain rate observed in the sample deformed at $\sim 2100 \text{ K}$ (run Beta037). According to the atomic diffusion data, Si is the slowest diffusion element among major elements in wadsleyite so that

Si is considered the rate-controlling species of deformation. The estimated creep strength of diffusion creep is compared with the observed data in Figure 8 and the strength with observed grain size of $0.5\text{--}1 \mu\text{m}$ is comparable with observed creep strength. This result indicates that the deformation in the experiment at $\sim 2100 \text{ K}$ might be controlled by diffusion creep.

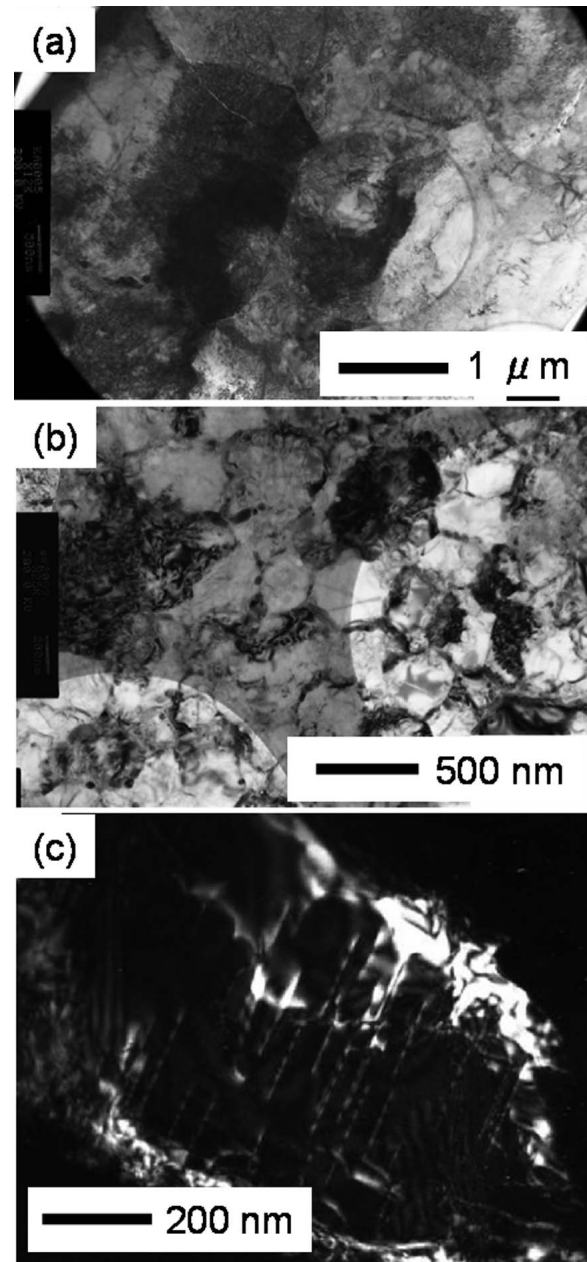


Figure 10. Transmission electron microscopy (TEM) images of the recovered sample deformed at 2030 K, 14.7 GPa, and $2.6 \times 10^{-5} \text{ s}^{-1}$ (run Beta035). (a and b) Heavily tangled dislocations are typical, forming subgrain boundaries. The size of cell structures varies from place to place. The cell size is around $400\text{--}500 \text{ nm}$. (c) Weak-beam dark field image of the subgrain with a lower dislocation density. The straight dislocations are typical and similar to the results by Thurel and Cordier [2003] and Thurel *et al.* [2003a].

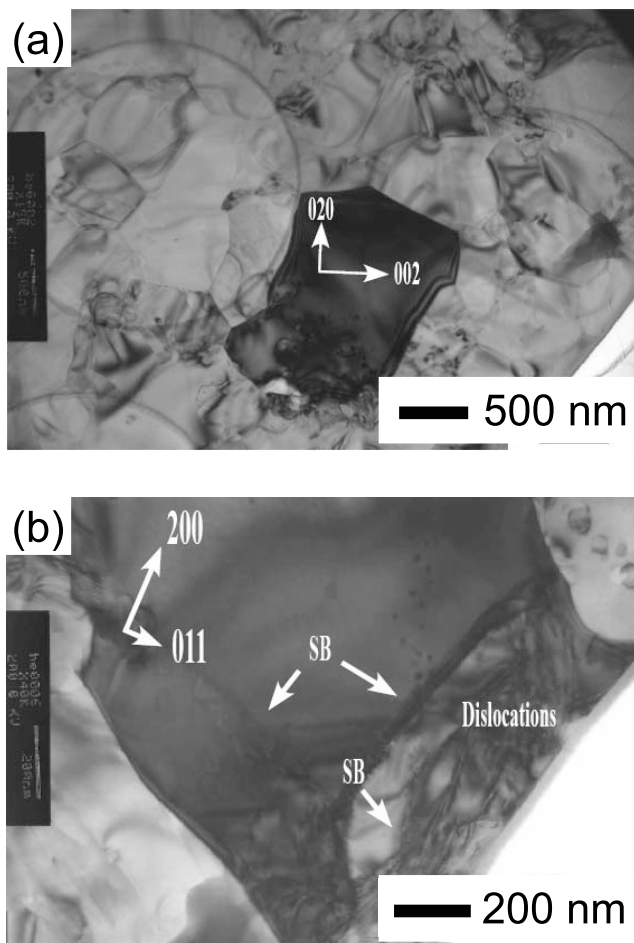


Figure 11. TEM images of recrystallized part of the recovered sample deformed at 2100 K, 17.0 GPa and $3.8 \times 10^{-5} \text{ s}^{-1}$ (run Beta037). (a) Dynamically recrystallized grains. The grains are basically dislocations free. (b) A few grains contain free dislocations and subgrain boundaries (SB) which are probably formed during dislocation creep.

[30] The creep strength data observed in this study are compared with previous results of wadsleyite at relatively dry conditions in Figure 8. The creep strengths observed at 1690 and 1930 K in this study are comparable to data obtained at 1600 and 1800 K using RDA [Nishihara *et al.*, 2008]. The creep strength of dry and wet wadsleyite was studied at 0–10 GPa and 298–873 K using a cubic anvil apparatus and in situ X-ray measurement [Chen *et al.*, 1998]. However, it is difficult to compare our data with the creep strength described by Chen *et al.* [1998] for the following reasons. The observed stress in the stress relaxation tests could be lower than that at steady state deformation because the magnitude of strain was too small to reach the steady state deformation. Also, the observed stress was measured by peak broadening method and could be overestimated due to effect of crushing of sample grains during compression process.

[31] In Figure 8, our results are also compared with creep strength of dry olivine in dislocation creep at 14 GPa from the extrapolation of low pressure (4.9–9.6 GPa) data on the basis of the value of activation volume determined by Kawazoe *et al.* [2009]. The creep strength of wadsleyite in this study

is comparable to that of dry olivine at a similar pressure within experimental errors. However, the water content is different between olivine and wadsleyite. If water content in olivine were increased to $\sim 2000 \text{ H}/10^6 \text{ Si}$, then the strength would be reduced by a factor of ~ 3 [e.g., Karato and Jung, 2003]. More detailed studies are needed to resolve the strength contrasts between olivine and wadsleyite.

5. Summary

[32] We have conducted deformation experiments of water-poor polycrystalline wadsleyite (water content, ~ 200 – $2200 \text{ H}/10^6 \text{ Si}$) under the transition zone conditions (pressures of 14.4–17.0 GPa up to temperatures of 2100 K) at strain rate of 2.6 – $16 \times 10^{-5} \text{ s}^{-1}$ to large strains. Deformation mechanisms at steady state are examined on the basis of the mechanical data determined by the synchrotron in situ X-ray observations as well as on the basis of microstructural observations. We identified two distinct regimes in plastic flow behavior. At low temperatures, the strength is insensitive to temperature and microstructural observations show no evidence for recovery. We suggest that the deformation occurs by dislocation glide alone without much recovery (i.e., the Peierls mechanism) in this regime. At higher temperatures, the strength is highly sensitive to temperature, and the microstructural observations show evidence of recovery and/or recrystallization. Some types of high-temperature creep mechanism operate in this regime, including dislocation and diffusion creeps. However, the exact mechanism of deformation is not well constrained from this study, because the detailed mechanical data such as the stress exponent was not determined. A comparison of strength of olivine and wadsleyite near the 410-km conditions shows similar strength, but the exact comparison is difficult at this stage because of the uncertainties in the influence of water and of grain size. The influence of stress and temperature are also not well constrained from the present study. Further studies in these directions are needed to improve our understanding of dynamics of the transition zone.

[33] **Acknowledgments.** This study has been supported by Consortium for Materials Properties Research in Earth Sciences (COMPRES) and by grants from the National Science Foundation. We appreciate the support of L. Wang, M. Vaughn, and C. Koleda, as well as D. J. Weidner for synchrotron experiments.

References

- Chen, J., T. Inoue, D. J. Weidner, Y. Wu, and M. T. Vaughan (1998), Strength and water weakening of mantle minerals, olivine, wadsleyite and ringwoodite, *Geophys. Res. Lett.*, *25*, 575–578, doi:10.1029/98GL00043.
- Chen, J. H., L. Li, D. Weidner, and M. Vaughan (2004), Deformation experiments using synchrotron X-rays: In situ stress and strain measurements at high pressure and temperature, *Phys. Earth Planet. Inter.*, *143*–*144*, 347–356, doi:10.1016/j.pepi.2003.09.021.
- Fei, Y., H. Mao, J. Shu, G. Parthasarathy, W. A. Bassett, and J. Ko (1992), Simultaneous high-P, high-T X ray diffraction study of β - $(\text{Mg,Fe})_2\text{SiO}_4$ to 26 GPa and 900 K, *J. Geophys. Res.*, *97*(B4), 4489–4495, doi:10.1029/92JB00076.
- Gasparik, T. (1996), Melting experiments on the enstatite-diopside join at 70–224 kbar, including the melting of diopside, *Contrib. Mineral. Petrol.*, *124*(2), 139–153, doi:10.1007/s004100050181.
- Hosoya, T., T. Kubo, E. Ohtani, A. Sano, and K. Funakoshi (2005), Water controls the fields of metastable olivine in cold subducting slabs, *Geophys. Res. Lett.*, *32*, L17305, doi:10.1029/2005GL023398.

- Karato, S. (2008), *Deformation of Earth Materials: Introduction to the Rheology of the Solid Earth*, 463 pp., Cambridge Univ. Press, Cambridge, U. K.
- Karato, S., and H. Jung (2003), Effects of pressure on high-temperature dislocation creep in olivine polycrystals, *Philos. Mag. A*, *83*, 401–414, doi:10.1080/0141861021000025829.
- Karato, S., and D. C. Rubie (1997), Toward experimental study of plastic deformation under deep mantle conditions: A new multianvil sample assembly for deformation experiments under high pressures and temperatures, *J. Geophys. Res.*, *102*(B9), 20,111–20,122, doi:10.1029/97JB01732.
- Kawazoe, T., S.-i. Karato, K. Otsuka, Z. Jing, and M. Mookherjee (2009), Shear deformation of dry polycrystalline olivine under deep upper mantle conditions using a rotational Drickamer apparatus (RDA), *Phys. Earth Planet. Inter.*, *174*(1–4), 128–137, doi:10.1016/j.pepi.2008.06.027.
- Kubo, T., E. Ohtani, and K. Funakoshi (2004a), Nucleation and growth kinetics of the α - β transformation in Mg_2SiO_4 determined by in situ synchrotron powder X-ray diffraction, *Am. Mineral.*, *89*(2–3), 285–293.
- Kubo, T., A. Shimojuku, and E. Ohtani (2004b), Mg-Fe interdiffusion rates in wadsleyite and the diffusivity jump at the 410-km discontinuity, *Phys. Chem. Miner.*, *31*, 456–464, doi:10.1007/s00269-004-0412-0.
- Li, B. S., R. C. Liebermann, and D. J. Weidner (2001), P-V-V-p-V-s-T measurements on wadsleyite to 7 GPa and 873 K: Implications for the 410-km seismic discontinuity, *J. Geophys. Res.*, *106*(B12), 30,579–30,591, doi:10.1029/2001JB000317.
- Mendelson, M. I. (1969), Average grain size in polycrystalline ceramics, *J. Am. Ceram. Soc.*, *55*, 19–24.
- Nishihara, Y., T. Shinmei, and S. Karato (2006), Grain-growth kinetics in wadsleyite: Effects of chemical environment, *Phys. Earth Planet. Inter.*, *154*(1), 30–43, doi:10.1016/j.pepi.2005.08.002.
- Nishihara, Y., D. Tinker, T. Kawazoe, Y. Xu, Z. Jing, K. N. Matsukage, and S.-i. Karato (2008), Plastic deformation of wadsleyite and olivine at high-pressure and high-temperature using a rotational Drickamer apparatus (RDA), *Phys. Earth Planet. Inter.*, *170*(3–4), 156–169, doi:10.1016/j.pepi.2008.03.003.
- Odqvist, F. K. G., and J. Hult (1962), *Kriechfestigkeit Metallischer Werkstoffe*, Springer, Berlin, Germany.
- Paterson, M. S. (1982), The determination of hydroxyl by infrared absorption in quartz, silicate glass and similar materials, *Bull. Mineral.*, *105*, 20–29.
- Rubie, D. C., and C. R. Ross II (1994), Kinetics of the olivine-spinel transformation in subducting lithosphere: Experimental constraints and implications for deep slab processes, *Phys. Earth Planet. Inter.*, *86*, 223–243, doi:10.1016/0031-9201(94)05070-8.
- Shimojuku, A., T. Kubo, E. Ohtani, and H. Yurimoto (2004), Silicon self-diffusion in wadsleyite: Implication for rheology of the mantle transition zone and subducting slabs, *Geophys. Res. Lett.*, *31*, L13606, doi:10.1029/2004GL020002.
- Shimojuku, A., T. Kubo, E. Ohtani, T. Nakamura, R. Okazaki, R. Dohmen, and S. Chakraborty (2009), Si and O diffusion in $(\text{Mg,Fe})_2\text{SiO}_4$ wadsleyite and ringwoodite and its implications for the rheology of the mantle transition zone, *Earth Planet. Sci. Lett.*, *284*(1–2), 103–112, doi:10.1016/j.epsl.2009.04.014.
- Singh, A. K. (1993), The lattice strain in a specimen (cubic system) compressed nonhydrostatically in an opposed anvil device, *J. Appl. Phys.*, *73*, 4278–4286, doi:10.1063/1.352809.
- Thurel, E., and P. Cordier (2003), Plastic deformation of wadsleyite: I. High-pressure deformation in compression, *Phys. Chem. Miner.*, *30*, 256–266.
- Thurel, E., P. Cordier, D. J. Frost, and S. Karato (2003a), Plastic deformation of wadsleyite: II. High-pressure deformation in shear, *Phys. Chem. Miner.*, *30*, 267–270.
- Thurel, E., J. Douin, and P. Cordier (2003b), Plastic deformation of wadsleyite: III. Interpretation of dislocation slip systems, *Phys. Chem. Miner.*, *30*, 271–279.
- Xu, Y., Y. Nishihara, and S. Karato (2005), Development of a rotational Drickamer apparatus for large-strain deformation experiments under deep Earth conditions, in *Frontiers in High-Pressure Research: Applications to Geophysics*, edited by J. Chen et al., pp. 167–182, doi:10.1016/B978-044451979-5/50010-7, Elsevier, Amsterdam.

J. Ando, Department of Earth and Planetary Systems Science, Hiroshima University, 1-3-1 Kagamiyama, Higashihiroshima, Hiroshima 739-8526, Japan.

J. W. Hustoft, Z. Jing, S. Karato, T. Kawazoe, and K. Otsuka, Department of Geology and Geophysics, Yale University, 210 Whitney Avenue, New Haven, CT 06511, USA. (kawazoe@sci.chime-u.ac.jp)